Unplugging DI-DIV and DII-DIII lateral fenestrations of NALCN reveals unexpected pharmacology

Katharina Schott, Stephan Alexander Pless, Han Chow Chua*#

Department of Drug Design and Pharmacology, University of Copenhagen, Jagtvej 160, 2100 Copenhagen, Denmark.

*Corresponding author. Email: chow.chua@sydney.edu.au

#Current address: A15 Pharmacy and Bank Building, Science Road, The University of Sydney 2006 Camperdown, Sydney, Australia.

Abstract

The sodium (Na^+) leak channel (NALCN) is a member of the four-domain voltage-gated cation channel family that includes the prototypical voltage-gated sodium and calcium channels (Na_VS and Ca_VS, respectively). Unlike Na_VS and Ca_VS, which have four intramembrane fenestrations that serve as routes for lipophilic compounds to enter the central cavity to modulate channel function, NALCN has bulky residues (W311, L588, M1145 and Y1436) that block these openings. Structural data suggest that occluded lateral fenestrations underlie the pharmacological resistance of NALCN, but functional evidence is lacking. To test this hypothesis, we unplugged the fenestrations of NALCN by substituting the four aforementioned residues with alanine (AAAA) and compared the effects of Na_V, Ca_V and NALCN blockers on both wild-type (WT) and AAAA channels. Most compounds behaved in a similar manner on both channels, but phenytoin and 2-aminoethoxydiphenyl borate (2-APB) elicited additional, distinct responses on AAAA channels, highlighting the existence of drug binding sites beyond the occluded fenestrations of NALCN. Further experiments using single alanine mutants revealed that phenytoin and 2-APB access their putative binding sites through distinct fenestrations, implying structural specificity to their modes of access. Intrigued by the activity of 2-APB and its analogues, we tested more compounds containing the diphenylmethane/amine moiety on WT channels. We identified novel compounds that exhibited diverse activity, thus expanding the pharmacological toolbox for NALCN. While the low potencies of active compounds reiterate the resistance of NALCN to pharmacological targeting, our findings lay the foundation for rational drug design to develop NALCN modulators with refined properties.

Introduction

NALCN mediates a tonic Na^+ conductance that contributes to the resting membrane potential (RMP) of excitable and non-excitable cells. Over the last two decades, animal studies have shown that NALCN function regulates various bodily processes such as respiration, motor function, pain sensitivity, circadian rhythm and cancer metastasis (1-9). In humans, dysfunction that arises from NALCN mutations has detrimental effects on health. Evidence from clinical studies indicates that *de novo* missense mutations can cause congenital contractures of the limbs and face, resulting in characteristic facial features, hypotonia and variable degrees of developmental delay (CLIFAHDD), whereas homozygous mutations are linked to infantile hypotonia with psychomotor retardation and characteristic facies (IHPRF1) (10-14). The physiological significance of NALCN has garnered much interest in the ion channel field, but challenges associated with functional expression have left NALCN lagging considerably behind other closely related channels in terms of the understanding of its structure, function and pharmacology (15-18).

As a member of the four-domain voltage-gated cation channel family, NALCN shares a common topology with the prototypical Navs and Cavs. These large membrane proteins are composed of four homologous but non-identical domains connected via intracellular linkers. Each of the four domains (DI–DIV) contains six transmembrane segments (S1–S6), with S1–S4 forming the voltage-sensing domains (VSDs) and S5–S6 forming the pore domains (PDs). The four VSDs are situated peripherally to a central ion-conducting pore, working in concert to couple membrane depolarisation to cation influx. Despite the conserved channel architectur, NALCN stands out from Navs and Cavs due to its unusual functional and pharmacological profiles. First, a prerequisite for NALCN function is the formation of a massive channelosome with three non-conducting auxiliary subunits: uncoordinated protein 79 (UNC79), uncoordinated protein 80 (UNC80) and family with sequence similarity 155 member A (FAM155A, also known as NALCN auxiliary factor 1 (NALF1)) (19, 20). Second, while canonical Navs and Cavs cycle between distinct closed, activated and inactivated states in response to hyperpolarisation and depolarisation of the membrane potential, NALCN shows constitutive activity that is modulated by voltage and extracellular divalent cations (19). Third, NALCN exhibits strikingly low open channel probability (P_O) even during periods of high activity (P_O~0.04 at -60 mV) (21). Fourth, NALCN is resistant to pharmacological targeting,

with the most potent inhibitor known to date being the trivalent cation gadolinium (Gd^{3+}), a promiscuous inhibitor of miscellaneous ion channels including Na_Vs, Ca_Vs, mechanosensitive, stretch-activated and transient receptor potential (TRP) channels (1, 19, 22).

In stark contrast to the lack of NALCN-specific pharmacology, Na_Vs and Ca_Vs are modulated by a vast array of natural and synthetic compounds. Animal and plant toxins generally inhibit Na_V and Ca_V function either by blocking the extracellular mouth of the ion permeation pathway or binding to the VSDs to modify channel gating (23-25). On the other hand, numerous lipophilic blockers travel across intramembrane lateral fenestrations that exist between specific interfaces of two adjacent PDs to directly occlude the central pore (**Fig. S1A**). An impressive list of clinically used drugs such as anaesthetic (e.g., lidocaine) (26), antiarrhythmic (e.g., flecainide) (27), antihypertensive and antianginal (e.g., verapamil and diltiazem) (28), antispasmodic (e.g., otinolium bromide) (29), and motion sickness drugs (e.g., cinnarizine) (30) enter the central cavity through these routes to inhibit Na_Vs and Ca_Vs. In addition, lateral fenestrations also house allosteric binding sites for inhibitors to negatively modulate channel function without directly blocking the pore. For example, dihydropyridine Ca_V blockers such as amlodipine and nifedipine bind to the fenestration between the PDs of DIII and DIV (the DIII-DIV fenestration) of $Ca_V1.1$ to inhibit channel function (28, 31). Lipids are also frequent occupants of the fenestrations, with evidence suggesting that they can modulate channel function and help coordinate binding of drugs (28, 29, 32-34). Taken together, lateral fenestrations are an integral structure feature of Na_Vs and Ca_Vs that serve both as key drug access pathways as well as drug binding sites.

Since 2020, we have seen the determination of multiple structures of the NALCN channelosome (21, 22, 35-38). This nearly one-megadalton complex includes (1) the membrane-embedded NALCN, (2) the auxiliary subunit FAM155A forming a dome that sits above the channel, and (3) UNC79 and UNC80 forming a massive, intertwined superhelical assembly that docks intracellularly to the bottom of NALCN (**Fig. S1B**). The extracellular dome of FAM155A has been postulated to physically prevent molecules from accessing the selectivity filter, which may explain the insensitivity of NALCN to toxins that rely on this route to inhibit related channels (22). Despite having a central cavity with comparable volume to the classical drug-receptor site in Na_Vs and Ca_Vs, four S6 residues (W311 of DI, L588 of DII, M1145 of DIII and Y1436 of DIV) appear to plug the lateral fenestrations in NALCN (**Fig.**

S3A). Based on this structural observation, an obvious question arises: could the occluded lateral fenestrations of NALCN serve as barricades to prevent drug entry, and hence contribute to the pharmacological resistance of this idiosyncratic channel? In this study, we sought to understand the impact of unplugging the lateral fenestrations on NALCN pharmacology and to expand the NALCN pharmacological toolbox.

Results

Alanine substitutions at the lateral gateways of NALCN widen fenestrations *in silico*

To identify the lateral fenestrations of NALCN or the lack thereof, we first subjected WT channel structure (PDB 7SX3) through an automatic tunnel detection software, MOLE 2.5 (See Materials and methods for details). While we did not identify a tunnel at the DIII-DIV interface, we found predicted lateral tunnels at the DI-DII, DII-DIII and DI-DIV interfaces of the WT channel. However, these tunnels were narrow (bottleneck radii of DI-DII=0.9 Å, DII-DIII=1.0 Å, DI-DIV=1.2 Å; **Fig. 1A**), echoing previous speculation that NALCN lacks lateral fenestrations that can serve as routes for small molecule entry into the central cavity (22). For comparison purposes, we also analysed apo structures of $Na_V1.5$ (PDB 6UZ3) and $Ca_V3.3$ (PDB 7WLI). Consistent with the idea that lipids and lipophilic compounds pass through the lateral fenestrations of these channels, we detected wider lateral tunnels (bottleneck radii > 2.0 Å) at most domain interfaces (**Fig. S1C**). Next, we substituted the four key bottleneck residues of each interface of NALCN (W311 of DI, L588 of DII, M1145 of DIII, and Y1436 of DIV) with alanine *in silico* (mutagenesis performed using Pymol) and applied the same analysis. This four-fold alanine (AAAA) mutant, in stark contrast to the WT channel, had lateral tunnels through DI-DII, DII-DIII, DIII-DIV and DI-DIV interfaces that were noticeably wider (**Fig. 1A)**. The DI-DIV fenestration had the largest bottleneck radius of 2.7 Å, followed by DII-DIII (2.5 Å), DIII-DIV (2.2 Å) and finally DI-DII, which was the narrowest with a bottleneck radius of 1.7 Å. A simple interpretation of these results is that the four-fold alanine substitution widened the lateral fenestrations of NALCN, with two out of the four potential fenestrations (DII-DIII and DI-DIV) having radii wide enough to accommodate compound entry. To verify these predictions, we proceeded to evaluate the function and pharmacology of the AAAA channel *in vitro*.

Functional characterisation of the alanine mutants in *Xenopus laevis* oocytes

To determine the effect of these alanine mutations on channel function, we introduced single (W311A, L588A, M1145A and Y1436A) and four-fold alanine mutations into NALCN using site-directed mutagenesis and expressed these mutant channels with the auxiliary subunits UNC79, UNC80 and FAM155A in *Xenopus laevis* oocytes. We then measured voltage-evoked currents from each construct using the two-electrode voltage-clamp technique five days post RNA injection. As the NALCN channel complex is highly sensitive to inhibition by physiological concentrations of extracellular divalent cations such as Ca^{2+} and Mg^{2+}, we performed our recordings in Ca^{2+}- and Mg^{2+}-free buffer (substituted with Ba^{2+}). WT NALCN channel conducted robust currents in response to depolarisation and hyperpolarisation from a holding potential of 0 mV (4.4±0.9 µA at +80 mV; 2.6±1.0 µA at -80 mV; n=73; **Fig. 1B and C**). The AAAA mutant channel showed a small but significant decrease in current amplitudes (3.7±0.6 µA at +80 mV; 1.9±0.6 µA at -80 mV; n=75; p<0.0001; one-way ANOVA, Dunnett's test (compared to WT); **Fig. 1B and C**). The single W311A mutation unexpectedly resulted in markedly lower current amplitudes both in the outward and inward directions (1.9±0.5 µA at +80 mV; 0.6±0.1 µA at -80 mV; n=14; p<0.0001; one-way ANOVA, Dunnett's test (compared to WT); **Fig. 1B and C**). The remaining three single mutants L588A, M1145A and Y1436A behaved similarly to WT channels, with no significant differences in current amplitudes, except for a slight increase for Y1436A at hyperpolarised potentials (4.0±1.9 µA at -80 mV; n=14; p<0.0001; one-way ANOVA, Dunnett's test (compared to WT); **Fig. 1B and C**). We also observed apparent differences in the current deactivation kinetics in response to hyperpolarising voltage steps with some of the mutants (e.g., M1145A and Y1436A; **Fig. 1B**), but did not further investigate this effect.

Pharmacological screening reveals distinct responses for phenytoin and 2-APB on WT and AAAA channels

Having established that the AAAA mutant channel displayed WT-like function, we evaluated if the fenestrations or the central cavity of NALCN houses potential drug binding sites. We hypothesised that by widening the lateral fenestrations of NALCN, some compounds that are ineffective on WT channel would exert modulatory effect on the AAAA channel. Alternatively, previously reported inhibitors of NALCN may have increased potency or additional, previously unseen effects on the mutant channel. To test this hypothesis, we expressed both WT and

AAAA channel complexes in *Xenopus laevis* oocytes and then measured their responses to 13 lipophilic channel modulators. We chose these compounds either for their ability to enter Na_Vs or Ca_Vs via the lateral fenestrations or for their reported inhibitory effect on NALCN. Considering the pharmacological resistance of NALCN, we started testing each compound with the maximum soluble concentration achievable or 1 mM if solubility was not an issue (concentration range=100 µM to 1 mM).

Overall, the effects of these compounds on both WT and AAAA channels were diverse (**Fig. 2A and B**). Five out of the 13 compounds tested (carbamazepine, lidocaine, phenytoin, lacosamide, and Z944) showed no effect on WT channels; two selectively inhibited the outward (CP96345) or inward (lamotrigine) currents; three inhibited the outward and potentiated the inward currents (quinidine, diltiazem, and propafenone); three inhibited both outward and inward currents (nifedipine, L-703,606, and 2-APB). In addition to the effects on current amplitudes, we also observed changes in current phenotype. For example, the application of quinidine, diltiazem, propafenone and CP96435 resulted in a "hooked" current at hyperpolarized potentials, suggesting that these compounds may have an impact on channel gating (**Fig. 2A**).

The AAAA mutant channel responded similarly to the WT channel for most of these compounds, except for phenytoin and 2-APB. While the application of 300 µM phenytoin had no effect on WT channel currents, it significantly inhibited the inward current of AAAA channels (64.8±6.7 % inhibition at -100 mV; n=13; p<0.0001; one-way ANOVA, Dunnett's test (compared to WT); **Fig. 2A and B**). We have previously reported the inhibitory effect of 2-APB on NALCN (22). On WT channels, 1 mM 2-APB had a more prominent effect on inward (70.2±8.2 % inhibition at -100 mV; n=17) than outward current (23.2±26.7 % inhibition at +80 mV). The blocking effect of 2-APB was reversible, evident from the full recovery of currents after washout for two minutes (**Fig. 2A**). By contrast, 1 mM 2-APB only weakly inhibited the inward current of the AAAA mutant (32.9±12.9 % inhibition at -100 mV; n=21; **Fig. 2B**). We also occasionally observed slight activation of the outward current (30.5±27.0 % of activation at +80 mV). To our surprise, following the removal of 2-APB with a two-minute washout, the AAAA mutant channel showed even greater activation in both inward (167.9±50.3 %) and outward (227.7±122.4 %) directions.

Phenytoin inhibits M1145A and 2-APB activates W311A

To determine if phenytoin and 2-APB elicited their unique responses at AAAA channels via specific lateral fenestrations, we tested these compounds on individual alanine mutants. Like WT channels, the W311A, L588A and Y1436A mutants did not react to 300 µM phenytoin (**Fig. 3A**). The M1145A mutant, on the other hand, showed noticeably reduced currents in response to phenytoin (31.0±9.2 % of inhibition at -100 mV; n=11; p<0.0001; one-way ANOVA, Dunnett's test (compared to WT); **Fig. 3A**). For 2-APB, the reversible inhibitory effect observed on WT channels (**Fig. 2**) was replicated with L588A, M1145A and Y1436A mutants (**Fig. 3B**). By contrast, 2-APB activated W311A readily during application (87.1±60.2 % and 143.3±92.5 % of activation at +80 and -100 mV, respectively; n=9; **Fig. 3B**). This stimulatory effect was even more pronounced post washout, with 334.6±146.6 % and 484.0±238.7 % of activation measured at +80 and -100 mV, respectively. Taken together, these results suggest that these compounds access their putative binding site(s) via different lateral fenestrations, with phenytoin and 2-APB likely using the DII-DIII and DI-DIV fenestrations, respectively.

Reintroduction of a bulky residue at the DI-DIV fenestration prevents 2-APB activation

Our computational data suggest that the W311A mutation widens the DI-DIV fenestration (**Fig. 1A**). If a wider DI-DIV fenestration was directly responsible for the 2-APB activation observed at W311A and AAAA, we hypothesised that reintroducing a bulky residue at the DI-DIV interface of the W311A mutant should prevent 2-APB entry and activation. For this purpose, we generated two new mutants W311F and W311A/L1439W. These mutants had narrower predicted tunnels at the DI-DIV interface (bottleneck radii of 1.3 and 1.6 Å for W311F and W311A/L1439W, respectively; **Fig. S2**). Like W311A, both mutants showed reduced current amplitudes compared to WT, suggesting that tryptophan at position 311 plays a critical role for channel function as even a subtle tryptophan-to-phenylalanine substitution was not well tolerated. The application and subsequent removal of 2-APB, however, did not result in current activation at these mutants (**Fig. 3B**), supporting our speculation that 2-APB is able to enter and bind to a previously inaccessible activation site only when we unplugged the DI-DIV fenestration with the W311A mutation.

Inhibition masks activation during 2-APB application

We were interested in the activation effect of 2-APB at W311A and AAAA channels, but our standard recording protocol did not determine the reversibility and time-course of the activation effect. To this end, we repeated the 2-APB experiments on the AAAA mutant but measured currents in two-minute intervals after the first washout to determine the time required for currents to return to baseline. We found that, despite the removal of 2-APB, the activating effect persisted, and it took as long as eight minutes for the current responses to gradually return to baseline (**Fig. 3C**, left panel). This sustained activation effect contrasts with the quick washout of the inhibitory effect observed with WT channels (**Fig. 2A**) and indicates the potential existence of an intramembrane activation site for 2-APB. In a separate experiment, we reapplied 2-APB for 30 seconds immediately after the two-minute washout period, and observed the activated current returned to baseline levels (**Fig. 3C**, right panel). These data suggest that inhibition and activation occurred simultaneously during 2-APB perfusion, and that the weakened inhibition and occasional slight activation observed following application of 2-APB at W311A and AAAA channels was a net result of the two opposing effects (**Fig. 2A and 3B**).

Effects of different 2-APB analogues on NALCN currents

Owing to the ability of 2-APB to form a nitrogen-to-boron coordinate covalent bond, the molecule can exist in different forms including a ring form, an open chain form or a dimeric form (**Fig. 4A**) (39). Our data already showed that phenytoin, a structural analogue of the ring form, did not have any effect on NALCN current even when applied at concentration as high as 300 μM (**Fig. 2 and 4B**). Considering the ability of 2-APB to switch between its different forms, we investigated which form(s) of 2-APB were responsible for the inhibition of WT currents. We therefore tested the effects of two 2-APB analogues on WT channels. The antihistamine diphenhydramine resembles the open chain form of 2-APB (**Fig. 4A**). At 1 mM, diphenhydramine inhibited the outward current (60.3±4.3 % of inhibition at +80 mV; n=9; **Fig. 4B**) and activated the inward current (84.9±19.8 % of activation at -100 mV; n=9; **Fig.4B**). The dimeric analogue diphenylboronic anhydride (DPBA), on the other hand, inhibited NALCN current in both directions with higher efficacy than 2-APB at 1 mM (66.9±4.0 % and 79±6.1 % of inhibition at +80 and -100 mV, respectively; n=7; p<0.0001; one-way ANOVA, Dunnett's test (compared to 2-APB); **Fig. 4B**).

Functional screening of compounds containing the diphenylmethane/amine motif

Up until this point, we found only three small molecules that have strong inhibitory effect on WT channel, namely L-703,606, 2-APB and DPBA (~70–80 % of inward current inhibition at -100 mV; **Fig. 2B and 4B**). However, none of these compounds had potency comparable to that of the trivalent cation Gd^{3+}. Since a common feature of these compounds is the diphenyl-x (x=carbon/boron) motif, we tested if other small molecule drugs with similar feature also modulate NALCN function. For this purpose, we tested nine compounds that have the diphenylmethane/amine motif including antihistamines (hydroxyzine, cetirizine, lomerizine and promethazine), antidepressants (citalopram), cognitive-enhancing drugs (linopirdine), anticancers ((E/Z)-endoxifen), statins (fluvastatin) and pharmacological tools (ICA-121431, a potent blocker of $Na_V1.1$ and $Na_V1.3$). We found that three compounds (lomerizine, ICA-121431 and linopirdine) had little to no effect on NALCN when applied at 100 μM (**Fig. 4D**), three (hydroxyzine, promethazine and citalopram) had a stronger inhibitory effect on the outward than inward current, two (cetirizine and (E/Z)-endoxifen) inhibited both outward and inward currents, and one (fluvastatin) had no effect on the outward current, but inhibited the inward current efficaciously. These data suggest that the diphenyl-x (x=carbon/boron/nitrogen) motif may be a promising starting point for future structure-activity relationship studies.

Discussion

In 1977, in an attempt to explain the ability of neutral local anaesthetics to inhibit Na_VS even when the intracellular gate is closed, Hille proposed that there are alternative hydrophobic pathways in the membrane for lipid-soluble blockers to “come and go from the receptor” (40). The existence of such pathways has since been overwhelmingly supported by functional, structural and computational studies (26, 29, 33, 41-44). In eukaryotic Na_VS and Ca_VS, four lateral fenestrations that extend from the cell membrane to the inner pore exist at the interfaces between the S5 and S6 helices of neighbouring PDs (DI-DIV, DI-DII, DII-DIII and DIII-DIV; **Fig. S1A**) (45). These fenestrations are hydrophobic in nature and the physical dimensions of each fenestration are unique and dynamic, as they change depending on the functional state of the channel and the presence of lipids or inhibitors (44, 46-48). Functionally, these side passages serve both as routes for lipids and lipophilic molecules to enter or leave the central

cavity and as allosteric binding sites. Additionally, they are potential sites for drug-drug interactions, as exemplified by the concomitant use of the antiarrhythmic agent amiodarone and the antiviral sofosbuvir. Amiodarone inhibits Ca_V function by binding to the DIII-DIV fenestrations of the Ca_V1 subfamily members, but its binding unexpectedly helps anchor the binding of sofosbuvir in the central cavity, leading to synergistic pore block and fatal heartbeat slowing (49). There is also increasing appreciation for the pathophysiological relevance of lateral fenestrations following reports of disease mutations identified in this region of Na_Vs (45). These mutations not only affect intrinsic channel function, but also alter the physical and/or chemical nature of these fenestrations, which may in turn affect drug accessibility via these routes. Hence, a detailed understanding of the properties and druggability of these often-overlooked side passages will help elucidate their roles in diseases and their potential exploitation in clinical or medical settings.

Potential drug binding sites in and beyond the plugged lateral fenestrations of NALCN

Thus far, all six available structures of NALCN indicate a lack of accessible lateral fenestrations, which is evident from their narrow bottleneck radii and the absence of resolved lipid molecule densities in this region (21, 22, 35-38). Given that lateral fenestrations contribute immensely to the pharmacology of the four-domain voltage-gated cation channel family, we hypothesised that the lack of lateral fenestrations may contribute to the pharmacological resistance of NALCN. Here, we demonstrate that substituting key bulky bottleneck residues that block these fenestrations in NALCN with alanine, which possesses a smaller side chain, renders the mutant channels sensitive to pharmacological effects not observed with WT channels. A particularly striking example is phenytoin, which clearly inhibits inward currents of AAAA channels, but has negligible activity on WT channels (**Fig. 2A and B**). On the other hand, 2-APB inhibits both WT and AAAA channels, but is also able to activate AAAA channels simultaneously. These data are consistent with our hypothesis: plugged lateral fenestrations contribute to the pharmacological resistance of NALCN, and freeing up these blocked routes allows drug entry, resulting in new pharmacological effects. An enticing implication of these results is that there are potential drug binding sites in and beyond the plugged lateral fenestrations of NALCN that are inaccessible in WT channels. We believe this is plausible for two reasons: first, NALCN has a central cavity of sufficient volume to accommodate Na_V and Ca_V ligands that bind in this region (22), and second, while the overall degree of sequence conservation between NALCN and other members in the same superfamily

342 is low, some residues implicated in drug binding within the central cavity of Na$_V$s and Ca$_V$s
343 are conserved in NALCN (e.g., Y1365 and A1369 on S6-DIV of Ca$_V$1.1 important for
344 verapamil and diltiazem binding; **Fig. S2**). Taken together, our data suggest that the plugged
345 lateral fenestrations in NALCN contribute to its pharmacological resistance, potentially by
346 guarding druggable sites in the central cavity.

347

348 **Phenytoin and 2-APB exert their unique effects via different fenestrations**

349 There are now multiple lines of evidence in support of the idea that drugs access their
350 intramembrane binding sites in Na$_V$s and Ca$_V$s in a domain interface-dependent manner (**Fig.**
351 **S1A**). Various clinical and pharmacological compounds have been detected in specific
352 individual fenestrations of Na$_V$ and Ca$_V$ cryo-EM structures (e.g., bulleyaconitine A: DI-DII of
353 Na$_V$1.3; flecainide: DII-DIII of Na$_V$1.5; nifedipine: DIII-DIV of Ca$_V$1.1; A-803467: DI-DIV
354 of Na$_V$1.8; **Fig. S1A**) (27, 28, 50, 51). Although compound concentrations used in sample
355 preparation can go up to several hundred-fold higher than their potencies, these findings
356 indicate the specificity of the interactions between compounds and individual fenestrations.
357 Metadynamics simulations performed on Na$_V$ structures concur with structural studies by
358 demonstrating that the local anaesthetic lidocaine prefers to pass through the DI-DII
359 fenestration to achieve its pore-blocking effect (42). To determine if phenytoin and 2-APB
360 have preferred entry route(s) at the AAAA mutant, we tested the effects of both compounds at
361 single alanine mutant channels that have only one fenestration unplugged at a time. Our results
362 show that phenytoin selectively inhibits the single M1145A mutant (**Fig. 3A**), whereas 2-APB
363 selectively activates the single W311A mutant (**Fig. 3B**). These findings are in line with
364 phenytoin and 2-APB favouring the DII-DIII and DI-DIV fenestrations, respectively, which
365 are the widest fenestrations based on our *in silico* predictions (**Fig. 1A**).

366

367 **The existence of two distinct binding site(s) for 2-APB at AAAA channels**

368 The synthetic compound 2-APB is a membrane-permeable, multi-target modulator that inhibits
369 inositol 1,4,5-trisphosphate (IP3) receptors (52), activates two-pore potassium (K2P) channels
370 (53), and inhibits/activates Ca^{2+} release-activated Ca^{2+} (CRAC) channels (54) and different
371 members of the Transient Receptor Potential (TRP) channel family (55). We have previously
372 reported 2-APB as a low-potency inhibitor of NALCN (22). In this study, we also find that 2-
373 APB activates NALCN efficaciously when the DI-DIV fenestration is unplugged (**Fig. 2A and**

3B). To explain our functional data, we propose a two-site model for 2-APB in which the inhibitory binding site(s) are found on the extracellular side of NALCN, whereas the activation site(s) are in the DI-DIV lateral fenestration (**Fig. 3D**). During 2-APB application, the compound binds simultaneously to the inhibitory and activation sites at the AAAA or W311A mutant, providing an explanation for the masked activation effect of 2-APB during drug application. Next, following drug removal with a two-minute buffer washout, 2-APB leaves the extracellular inhibitory site rapidly. However, 2-APB stays bound at the activation site due to the lipophilicity of both compound and fenestration, rationalising the prominent and long-lasting agonist response after washout (**Fig. 3C**). In support of this model, reintroduction of a bulky residue in the DI-DIV lateral portal (as in the case of W311F and W311A/L1439W mutants) prevents 2-APB activation (**Fig. 3B**), likely by blocking 2-APB entry into the DI–DIV fenestration. It is worth noting that the existence of multiple 2-APB binding sites, both in the extracellular and intramembrane space, have been found on members of the TRP channel family, which share similar channel architecture as Na$_V$s, Ca$_V$s and NALCN (55). While these findings are not direct evidence in support of our two-site model at NALCN, the ability of 2-APB to access spatially distinct sites is not unexpected given its promiscuity and membrane permeability.

Physiological implications

Our study has illustrated that there is potential pharmacology to be exploited beyond the occluded fenestrations of NALCN. While we have achieved this artificially by reducing the side-chain volume of key bottleneck residues with alanine substitutions, it is possible that the fenestration-plugging residues may adopt different conformations, which in turn could alter the radii and accessibility of these fenestrations. In fact, there is structural evidence supported by molecular dynamics (MD) simulations that key aromatic residues along lateral fenestrations of prokaryotic and eukaryotic Na$_V$s are mobile and their distinct rotamer conformations can directly gate the fenestration openings. For instance, the highly conserved phenylalanine residue in the middle of S6-DI (position 15) of Na$_V$1.7 (absolutely conserved in all Na$_V$s and Ca$_V$s; corresponds to W311 of NALCN; **Fig. S2**) can adopt a downward or an upward configuration (when viewed from the side of the membrane), depending on local conformational changes in the PDs (**Fig. S3B**) (44, 56). As such, the side chain movements of this critical phenylalanine residue will widen (downward) or narrow (upward) the bottleneck radius of the DI-DIV fenestration of Na$_V$1.7. In agreement with these observations, MD

simulations consistently identify this phenylalanine as a key bottleneck residue across different Na_V subtypes, and the mobility of these residues can have dramatic effect on fenestration dimensions (42). Therefore, although static snapshots of NALCN structures show that the lateral fenestrations at all domain interfaces are sealed by bulky residues adopting an upward configuration (**Fig. S3A**), it is conceivable that these residues can transition to a downward position and open individual fenestrations sporadically under specific conditions. Some possibilities include ligand binding or oscillation between distinct functional states (which are yet unclear for NALCN) that would expectedly trigger local conformational changes in the PDs.

The possibility of disease mutations affecting fenestration dimensions of NALCN should also be considered when interpreting our mutational data. Out of the <50 *de novo* NALCN missense mutations reported to date, there are at least two (T513N of S5-DII and F1141V of S6-DIII) that occur at residues lining the lateral fenestrations of NALCN (**Fig. 1A**). These mutations are found in the DII-DIII fenestration of NALCN and given the close vicinity of F1141 to the key bottleneck residue M1145, we expect the Phe-to-Val substitution would enlarge the fenestration portal. However, predicted tunnels through the DII-DIII interface of either T513N or F1141V are not dissimilar to that of WT, as L591 and M1145 are still restricting access (**Fig. S3C**). Nonetheless, it is worth nothing that mutations of many adjacent residues including but not limited to L312I/V, V313G, F512V, L590F, V595F and L1150V have been identified in CLIFAHDD patients. As many of these *de novo* variants have drastic impact on channel function (22), it is reasonable to expect that these mutations may alter fenestration dimensions by perturbing the conformational landscape. We have also searched for naturally occurring NALCN variants in the gnomAD database but did not find any mutations affecting key bottleneck residues, which may reflect a physiological requirement for these fenestration-defining residues to remain unchanged. This is conjecturally supported by our functional data that modifications in these fenestrations, for instance at position 311, can have dramatic impact on NALCN function and pharmacology (W311A/F; **Fig. 1B and 3B**). As the study of NALCN channelopathies is still a growing field, the pathophysiological relevance of these fenestrations will hopefully become clearer in the future when more patient data become available.

Limitations and future directions

The first limitation of this study is that our hypotheses are guided predominantly by the currently available structural information. We have identified and mutated four key residues that appear to plug individual lateral fenestrations based on cryo-EM structures of NALCN. As proteins are dynamic entities, these static snapshots of NALCN do not report on the dynamics of fenestration dimensions. A potential issue with this approach is that residues at positions other than W311, L588, M1145 and Y1436 may take over the role of key bottleneck residues over time under different functional states. It is therefore important for future studies to use equilibrium simulations to understand the motions of fenestration-lining residues and how their conformations regulate the radii of these fenestrations. In addition, it is important to examine if small molecules can pass through the lateral fenestrations and if there are potential binding sites within the fenestrations and central cavity of NALCN. Functional validation of residues identified from MD studies will improve our understanding of these intricate side passages that can serve as foundation to evaluate their druggability in the future. The determination of open-state or gain/loss-of-function disease mutant structures of NALCN may provide further insights into the conformational flexibility of key bottleneck residues.

The second limitation lies in the small panel of 24 compounds screened on NALCN currents. While we identified compounds such as DPBA and fluvastatin as novel efficacious inhibitors of inward current of NALCN, their minimal effective concentrations are too high (100 μM to 1 mM) for them to be considered NALCN-specific blockers. To establish a clear structure-activity relationship, it is necessary to perform high-throughput screening to gather sufficient data. However, the constitutive activity of NALCN and its absolute requirement for three auxiliary subunits to function impose significant technical barriers at every step of this process, from the generation of stable cell lines to distinguishing NALCN-mediated current from non-specific leak during electrophysiological experiments. An alternative approach is to synthesise and characterise a library of structural analogues of hit compounds from our work here (2-APB, DPBA, (E/Z)-endoxifen and fluvastatin) and other studies (e.g., L-703,606) (57). Finally, considering the remarkable resistance of NALCN to pharmacological modulation, combining computer-aided drug design with artificial intelligence may help to explore a vast chemical space to find novel, potent and specific NALCN blockers.

Concluding remarks

There has been enormous progress in our understanding of NALCN channelosome structure and function in the last few years, but the scarcity of NALCN-specific pharmacological tools remains a significant challenge in the field. Delineating the mechanisms underlying this pharmacological resistance is therefore crucial to unlocking NALCN's potential as a pharmacological and therapeutic target. In this study, we have explored the hypothesis that occluded lateral fenestrations contribute to pharmacological resistance of NALCN and our findings suggest that key bottleneck residues in this region deter drug accessibility. Despite the identification of new NALCN blockers, the low potencies of these compounds reiterate the difficulty in targeting this leak channel. Perhaps, exploring alternative strategies focusing on auxiliary subunits (UNC79, UNC80 and FAM155A) of the channelosome in the future may help overcome the present paucity in NALCN-specific modulators.

Figure legends

Figure 1. Unplugging lateral fenestrations of NALCN by substituting key bottleneck residues with alanine. (A) Predicted tunnels at (1) DI-DIV, (2) DI-DII, (3) DII-DIII and (4) DIII-DIV interfaces of NALCN WT (*left*) and AAAA (*right*) channels (top view). Key bottleneck and fenestration-lining residues are labelled. The bottleneck radius values for all detected tunnels are indicated accordingly. No predicted tunnels were found at the DIII-DIV interface of WT. (B) Representative current traces from *Xenopus laevis* oocytes expressing WT, AAAA or single alanine mutant complexes (+UNC79, UNC80 and FAM155A) in response to step protocols from +80 to −100 mV (holding potential, HP=0 mV) in Ca^{2+}- and Mg^{2+}-free buffer. (C) The plot shows current amplitudes elicited at +80 and -80 mV for all tested constructs. ****$p< 0.0001$ using one-way ANOVA, Dunnett's test (against WT). Dotted lines indicate the minimum and maximum current values of WT.

Figure 2. Effects of Nav, Cav and NALCN inhibitors at NALCN WT and AAAA channels. (A) Representative current traces from *Xenopus laevis* oocytes expressing WT or AAAA channel complexes (+UNC79, UNC80 and FAM155A) during control (black), compound application (red) and washout (blue) at +80 (outward) and -100 mV (inward) from a HP of 0 mV. (B) The plots show efficacy of different compounds at WT and AAAA channels during application (red) and washout (blue) normalised against control current at +80 mV (top) and -100 mV (bottom). ****$p< 0.0001$ using unpaired t-test.

Figure 3. Effects of phenytoin and 2-APB at single alanine NALCN mutants. (A–B) *Left*, representative current traces from *Xenopus laevis* oocytes showing the effects of 300 µM phenytoin (A) and 1 mM 2-APB (B) at various mutant channels in response to step protocols from +80 (outward) and −100 mV (inward) from a HP of 0 mV. *Right*, the plot shows percentage of current left during the application of phenytoin (A) or after the washout of 2-APB (B), normalised against control current elicited at -100 mV. (C) Representative current traces from *Xenopus laevis* oocytes expressing the AAAA mutant in response to application of 1 mM 2-APB using two protocols: *left*, single application of 2-APB (2) and currents measured at a 2-min interval for 8 min (3–6) during washout; *right*, 2-APB applied twice, before (2) and after (4) a single 2-min washout step (3). (D) Schematic of our proposed two-site model for 2-APB at NALCN channels containing the W311A mutation. ****$p< 0.0001$ using one-way ANOVA, Dunnett's test (against WT).

Figure 4. Effects of 2-APB analogues and compounds containing the diphenylmethane/amine motif at NALCN WT channels. (A) Different forms of 2-APB (*top*) and their corresponding structural analogues (*bottom*). (B) *Top,* representative current traces from *Xenopus laevis* oocytes expressing NALCN WT channel complex (+UNC79, UNC80 and FAM155A) in response to 1 mM 2-APB, 1 mM diphenhydramine (DPH), 300 µM phenytoin or 1 mM diphenylborinic anhydride (DPBA) at +80 mV (outward) and -100 mV (inward). *Bottom*, the plot shows percentage of current left during the application of 2-APB, DPH, phenytoin and DPBA. (C) Chemical structures of compounds containing the diphenylmethane/amine motif. (D) *Left*, representative current traces from *Xenopus laevis* oocytes expressing NALCN WT channel complex in response to different compounds (see Methods for concentrations tested). *Right*, the plots show efficacy of different compounds at

WT NALCN channels during application (red) and washout (blue) normalised against control current at +80 mV (top) and -100 mV (bottom).

Figure S1. (A) Top view of Na_V and Ca_V cryo-EM structures bound to blockers and phospholipids. (B) Side view of the NALCN channelosome structure. (C) Predicted lateral fenestrations of apo-$Na_V1.5$ (*top*) and apo-$Ca_V3.3$ (*bottom*) channels (top view). Bottleneck radii of individual predicted tunnels are indicated accordingly.

Figure S2. Sequence alignment of the pore segments of human NALCN, Nav and Cav channels. The residues involved in the binding and function of various compounds are shaded in different colours.

Figure S3. (A) Cartoon showing the upward configuration of key bottleneck residues in the lateral fenestrations of NALCN (side view). (B) Cartoon showing the flexible conformations of a highly conserved phenylalanine residue (F391) in S6-DI of $Na_V1.7$ (side view). F391 appears to adopt a downward configuration in the structure of $Na_V1.7$ WT in the absence of bound ligands (PDB 7W9K) and an upward configuration in the presence of the $Na_V1.7$ blocker XEN907 (PDB 7XM9). (C) Predicted tunnels at DII-DIII interface of NALCN T513N (*left*) and F1141V (*right*) channels (top view). Key bottleneck and fenestration-lining residues are labelled. The bottleneck radius values are indicated accordingly.

Materials and methods

Tunnel detection using MOLE 2.5

To prepare the WT channel structure for tunnel detection, we first removed the auxiliary subunits UNC79, UNC80, FAM155A and CaM from the channelosome structure (PDB 7SX3). We then used MOLE 2.5 (https://mole.upol.cz/) to detect tunnels in the structure of WT channel with default parameters as follows: minimal bottleneck radius 1.2 Å, probe radius 3 Å, surface cover radius 10 Å and origin radius 5 Å. We filtered out irrelevant tunnels that did not run parallel to the cell membrane and did not start from the central cavity. We used PyMOL to perform *in silico* mutagenesis on NALCN, and subjected mutant structures to the same procedure to detect lateral fenestrations.

Molecular biology

We cloned the human NALCN, UNC79, UNC80 and FAM155A complementary DNAs (cDNAs) between HindIII and XhoI sites in a modified pCDNA3.1(+) vector containing a 3′-*Xenopus* globin untranslated region and a polyadenylation signal. These constructs were generated using custom gene synthesis with codon optimization for *Homo sapiens* (GeneArt, Thermo Fisher Scientific). We generated all NALCN mutants using custom-designed primers (Eurofins Genomics or Merck) and PfuUltra II Fusion HS DNA Polymerase (Agilent Technologies) or the Q5 Site-Directed Mutagenesis Kit (New England Biolabs). We verified the sequences of plasmid DNAs purified from transformed *E. coli* by Sanger DNA sequencing (Eurofins Genomics). For expression in *Xenopus laevis* oocytes, we linearised plasmid DNAs with XbaI restriction enzyme, from which capped mRNAs were synthesised using the T7 mMessage mMachine Kit (Ambion).

Two-electrode voltage clamp

To surgically remove the ovarian lobes, adult female *X. laevis* were anaesthetized with 0.3% tricaine (under license 2014–15-0201–00031, approved by the Danish Veterinary and Food Administration). Frogs were housed and cared for by an animal facility approved by the University of Copenhagen. We then separated the ovarian lobes into smaller parts and defolliculated mechanically at 200 rpm at 37 °C. For injection, we sorted healthy-looking stage

V-VI oocytes. To prepare for injection, we diluted the mRNAs of NALCN (WT or mutant), UNC79, UNC80 and FAM115A to a concentration of 1000 ng/µL and then mixed in a ratio of 1:1:1:1. Using the Nanoliter 2010 injector (World Precision Instruments), we injected 36.8 or 41.4 nL of pre-mixed RNA into each oocyte. During injection, we lined up the oocytes in OR2 medium (82.5 mM NaCl, 2 mM KCl, 1 mM MgCl2, 5 mM HEPES) and injected the oocytes at the equator region of the cell. For optimal expression, we then incubated the oocytes at 140 rpm at 18 °C for 5 days in antibiotic medium (96 mM NaCl, 2 mM KCl, 1 mM MgCl2, 1.8 mM CaCl2, 5 mM HEPES, 2.5 mM pyruvate, 0.5 mM theophylline, 50 µg/mL gentamycin and tetracycline). We performed two-electrode-voltage clamp recordings using the OC-725C Oocyte Clamp amplifier (Warner Instrument Corp, USA). The microelectrodes (borosilicate glass capillaries, 1.2 mm OD, 0.94 mm ID, Harvard Apparatus) were pulled using the P-1000 horizontal puller (Sutter Instruments) and filled with 3 M KCl and had a resistance between 0.2-1.1 MΩ. Due to NALCN's sensitivity to the extracellular divalent cations Ca^{2+} and Mg^{2+}, the oocyte was constantly perfused with Ca^{2+}- and Mg^{2+}-free buffer that is substituted with Ba^{2+} [96 mM NaCl, 2 mM KCl, 1.8 mM $BaCl_2$ and 5 mM HEPES (pH 7.4) with NaOH], called Ca^{2+}/Mg^{2+}-free ND96. We acquired the data using the pCLAMP 10 software (Molecular Devices and a Digidata 1550 digitizer (Molecular devices), sampled at 10 kHz. We filtered electrical powerline interference with a Hum Bug 50/60 Hz Noise Eliminator (Quest Scientific).

For the pharmacological screening, we dissolved each tested compound to a stock solution in either Ca^{2+}/Mg^{2+}-free ND96 or DMSO, according to their solubility. We then diluted the stock solution further in Ca^{2+}/Mg^{2+}-free ND96. For the compounds that were only soluble in DMSO, the final DMSO concentration was kept at 1% or less. Due to NALCN's pharmacological resistance, we tested the compounds at the highest concentrations that were possible while maintaining the DMSO limit.

Final concentrations of compounds tested: 1 mM 2-APB (Sigma-Aldrich), 300 µM carbamazepine (VWR), 300 µM CP96345 (Tocris Bioscience), 300 µM diltiazem hydrochloride (Alomone Labs), 100 µM L-703,606 oxalate salt hydrate (Sigma-Aldrich), 300 µM lacosamide (Sigma Aldrich), 300 µM lamotrigine (Combi-Blocks), 300 µM lidocaine hydrochloride monohydrate (Sigma-Aldrich), 300 µM nifedipine (Alomone Labs), 300 µM

phenytoin sodium (VWR), 300 µM propafenone hydrochloride (Sigma-Aldrich), 300 µM quinidine (Sigma-Aldrich), 300 µM Z944 hydrochloride (Sigma-Aldrich), 1 mM diphenhydramine hydrochloride (Sigma-Aldrich), 1 mM diphenylborinic anhydride (DPBA; Sigma-Aldrich), 1 mM hydroxyzine dihydrochloride (Sigma-Aldrich), 1 mM cetirizine hydrochloride (Sigma-Aldrich), 100 µM lomerizine dihydrochloride (Sigma-Aldrich), 1 mM promethazine hydrochloride (Sigma-Aldrich), 1 mM citalopram hydrobromide (Sigma-Aldrich), 100 µM ICA-121431 (Sigma-Aldrich), 100 µM linopirdine (Sigma-Aldrich), 100 µM (E/Z)-endoxifen hydrochloride (Sigma-Aldrich) and 1 mM fluvastatin sodium (Sigma-Aldrich).

For the TEVC recordings, one oocyte (injected with either NALCN WT or mutant) was placed into the recording chamber with constant perfusion of Ca^{2+}/Mg^{2+}-free ND96. We then ran the first voltage protocol as a control and to check sufficient NALCN expression. Before testing compounds that were dissolved in a final DMSO concentration of 1%, we applied a Ca^{2+}/Mg^{2+}-free ND96 with 1 % DMSO control solution and ran the same voltage protocol to confirm that NALCN function was not affected by the DMSO content. Afterwards, we switched the perfusion in the recording chamber to the tested compound solution. To ensure that the oocyte was fully exposed to the compound, we perfused it with the compound solution for 30s and then ran the same voltage protocol again. To examine how long the effect of a compound lasted after it has been applied and washed-out, we switched the perfusion back to Ca^{2+}/Mg^{2+}-free ND96 and washed the oocyte for 2 min, followed by running the same protocol for a third time. To investigate the prolonged effect of 2-APB during wash-out, we continued constant perfusion with Ca^{2+}/Mg^{2+}-free ND96, running the same voltage protocol every 2 minutes.

Data analysis

We analysed the recorded currents using the Clampfit 10.7 software. The raw traces were filtered at 800 Hz (Gaussian low-pass filter) and representative current traces for illustration underwent data reduction with a reduction factor of 5. We performed statistical analysis using GrahPad Prism (Version 8.4, GraphPad Software), the specific statistical tests used are mentioned where relevant.

References

1. B. Lu *et al.*, The neuronal channel NALCN contributes resting sodium permeability and is required for normal respiratory rhythm. *Cell* **129**, 371-383 (2007).
2. H. A. Nash, R. L. Scott, B. C. Lear, R. Allada, An unusual cation channel mediates photic control of locomotion in *Drosophila*. *Curr Biol* **12**, 2152-2158 (2002).
3. E. Yeh *et al.*, A putative cation channel, NCA-1, and a novel protein, UNC-80, transmit neuronal activity in *C. elegans*. *PLoS Biol* **6**, e55 (2008).
4. L. Xie *et al.*, NLF-1 delivers a sodium leak channel to regulate neuronal excitability and modulate rhythmic locomotion. *Neuron* **77**, 1069-1082 (2013).
5. S. Gao *et al.*, The NCA sodium leak channel is required for persistent motor circuit activity that sustains locomotion. *Nat Commun* **6**, 6323 (2015).
6. O. Eigenbrod *et al.*, Rapid molecular evolution of pain insensitivity in multiple African rodents. *Science* **364**, 852-859 (2019).
7. B. C. Lear *et al.*, The ion channel narrow abdomen is critical for neural output of the *Drosophila* circadian pacemaker. *Neuron* **48**, 965-976 (2005).
8. M. Flourakis *et al.*, A conserved bicycle model for circadian clock control of membrane excitability. *Cell* **162**, 836-848 (2015).
9. E. P. Rahrmann *et al.*, The NALCN channel regulates metastasis and nonmalignant cell dissemination. *Nat Genet* **54**, 1827-1838 (2022).
10. M. D. Al-Sayed *et al.*, Mutations in NALCN cause an autosomal-recessive syndrome with severe hypotonia, speech impairment, and cognitive delay. *Am J Hum Genet* **93**, 721-726 (2013).
11. Ç. Köroğlu, M. Seven, A. Tolun, Recessive truncating NALCN mutation in infantile neuroaxonal dystrophy with facial dysmorphism. *J Med Genet* **50**, 515-520 (2013).
12. J. X. Chong *et al.*, *De novo* mutations in NALCN cause a syndrome characterized by congenital contractures of the limbs and face, hypotonia, and developmental delay. *Am J Hum Genet* **96**, 462-473 (2015).
13. T. Takenouchi *et al.*, Biallelic mutations in NALCN: Expanding the genotypic and phenotypic spectra of IHPRF1. *Am J Med Genet A* **176**, 431-437 (2018).
14. N. C. Bramswig *et al.*, Genetic variants in components of the NALCN-UNC80-UNC79 ion channel complex cause a broad clinical phenotype (NALCN channelopathies). *Hum Genet* **137**, 753-768 (2018).
15. J. H. Lee, L. L. Cribbs, E. Perez-Reyes, Cloning of a novel four repeat protein related to voltage-gated sodium and calcium channels. *FEBS Lett* **445**, 231-236 (1999).
16. L. A. Swayne *et al.*, The NALCN ion channel is activated by M3 muscarinic receptors in a pancreatic β-cell line. *EMBO Rep* **10**, 873-880 (2009).
17. A. N. Boone, A. Senatore, J. Chemin, A. Monteil, J. D. Spafford, Gd^{3+} and calcium sensitive, sodium leak currents are features of weak membrane-glass seals in patch clamp recordings. *PLoS One* **9**, e98808 (2014).
18. J. M. Egan, C. A. Peterson, W. M. Fry, Lack of current observed in HEK293 cells expressing NALCN channels. *Biochim Open* **6**, 24-28 (2018).
19. H. C. Chua, M. Wulf, C. Weidling, L. P. Rasmussen, S. A. Pless, The NALCN channel complex is voltage sensitive and directly modulated by extracellular calcium. *Sci Adv* **6**, eaaz3154 (2020).
20. M. Bouasse, H. Impheng, Z. Servant, P. Lory, A. Monteil, Functional expression of CLIFAHDD and IHPRF pathogenic variants of the NALCN channel in neuronal cells reveals both gain- and loss-of-function properties. *Sci Rep* **9**, 11791 (2019).
21. M. Kschonsak *et al.*, Structural architecture of the human NALCN channelosome. *Nature* **603**, 180-186 (2022).
22. M. Kschonsak *et al.*, Structure of the human sodium leak channel NALCN. *Nature* **587**, 313-318 (2020).
23. G. Wisedchaisri, T. M. Gamal El-Din, Druggability of voltage-gated sodium channels - Exploring old and new drug receptor sites. *Front Pharmacol* **13**, 858348 (2022).

24. W. A. Catterall, M. J. Lenaeus, T. M. Gamal El-Din, Structure and pharmacology of voltage-gated sodium and calcium channels. *Annu Rev Pharmacol Toxicol* **60**, 133-154 (2020).
25. D. Jiang, J. Zhang, Z. Xia, Structural advances in voltage-gated sodium channels. *Front Pharmacol* **13**, 908867 (2022).
26. T. M. Gamal El-Din, M. J. Lenaeus, N. Zheng, W. A. Catterall, Fenestrations control resting-state block of a voltage-gated sodium channel. *Proc Natl Acad Sci U S A* **115**, 13111-13116 (2018).
27. D. Jiang *et al.*, Structure of the cardiac sodium channel. *Cell* **180**, 122-134.e110 (2020).
28. Y. Zhao *et al.*, Molecular basis for ligand modulation of a mammalian voltage-gated Ca^{2+} channel. *Cell* **177**, 1495-1506.e1412 (2019).
29. L. He *et al.*, Structure, gating, and pharmacology of human $Ca_V3.3$ channel. *Nat Commun* **13**, 2084 (2022).
30. X. Yao, S. Gao, N. Yan, Structural basis for pore blockade of human voltage-gated calcium channel $Ca_V1.3$ by motion sickness drug cinnarizine. *Cell Res* **32**, 946-948 (2022).
31. S. Gao, N. Yan, Structural basis of the modulation of the voltage-gated calcium ion channel $Ca_V1.1$ by dihydropyridine compounds. *Angew Chem Int Ed Engl* **60**, 3131-3137 (2021).
32. Y. Zhao *et al.*, Cryo-EM structures of apo and antagonist-bound human $Ca_V3.1$. *Nature* **576**, 492-497 (2019).
33. X. Pan *et al.*, Structure of the human voltage-gated sodium channel $Na_V1.4$ in complex with β1. *Science* **362** (2018).
34. C. L. Noland *et al.*, Structure-guided unlocking of Na_X reveals a non-selective tetrodotoxin-sensitive cation channel. *Nat Commun* **13**, 1416 (2022).
35. J. Xie *et al.*, Structure of the human sodium leak channel NALCN in complex with FAM155A. *Nat Commun* **11**, 5831 (2020).
36. Y. Kang, J. X. Wu, L. Chen, Structure of voltage-modulated sodium-selective NALCN-FAM155A channel complex. *Nat Commun* **11**, 6199 (2020).
37. L. Zhou, H. Liu, Q. Zhao, J. Wu, Z. Yan, Architecture of the human NALCN channelosome. *Cell Discov* **8**, 33 (2022).
38. Y. Kang, L. Chen, Structure and mechanism of NALCN-FAM155A-UNC79-UNC80 channel complex. *Nat Commun* **13**, 2639 (2022).
39. C. K. Colton, M. X. Zhu, 2-Aminoethoxydiphenyl borate as a common activator of TRPV1, TRPV2, and TRPV3 channels. *Handb Exp Pharmacol* 10.1007/978-3-540-34891-7_10, 173-187 (2007).
40. B. Hille, Local anesthetics: hydrophilic and hydrophobic pathways for the drug-receptor reaction. *J Gen Physiol* **69**, 497-515 (1977).
41. M. R. Ghovanloo *et al.*, Cannabidiol inhibits the skeletal muscle $Na_V1.4$ by blocking its pore and by altering membrane elasticity. *J Gen Physiol* **153** (2021).
42. E. Tao, B. Corry, Characterizing fenestration size in sodium channel subtypes and their accessibility to inhibitors. *Biophys J* **121**, 193-206 (2022).
43. C. Boiteux *et al.*, Local anesthetic and antiepileptic drug access and binding to a bacterial voltage-gated sodium channel. *Proc Natl Acad Sci U S A* **111**, 13057-13062 (2014).
44. G. Huang *et al.*, High-resolution structures of human $Na_V1.7$ reveal gating modulation through α-π helical transition of S6(IV). *Cell Rep* **39**, 110735 (2022).
45. T. M. Gamal El-Din, M. J. Lenaeus, Fenestropathy of voltage-gated sodium channels. *Front Pharmacol* **13**, 842645 (2022).
46. D. Jiang *et al.*, Open-state structure and pore gating mechanism of the cardiac sodium channel. *Cell* **184**, 5151-5162.e5111 (2021).
47. J. Payandeh, T. M. Gamal El-Din, T. Scheuer, N. Zheng, W. A. Catterall, Crystal structure of a voltage-gated sodium channel in two potentially inactivated states. *Nature* **486**, 135-139 (2012).
48. W. A. Catterall, G. Wisedchaisri, N. Zheng, The conformational cycle of a prototypical voltage-gated sodium channel. *Nat Chem Biol* **16**, 1314-1320 (2020).
49. X. Yao *et al.*, Structural basis for the severe adverse interaction of sofosbuvir and amiodarone on L-type Ca_V channels. *Cell* **185**, 4801-4810.e4813 (2022).

50. X. Li *et al.*, Structural basis for modulation of human $Na_V1.3$ by clinical drug and selective antagonist. *Nat Commun* **13**, 1286 (2022).
51. X. Huang *et al.*, Structural basis for high-voltage activation and subtype-specific inhibition of human $Na_V1.8$. *Proc Natl Acad Sci U S A* **119**, e2208211119 (2022).
52. T. Maruyama, T. Kanaji, S. Nakade, T. Kanno, K. Mikoshiba, 2APB, 2-aminoethoxydiphenyl borate, a membrane-penetrable modulator of Ins(1,4,5)P3-induced Ca^{2+} release. *J Biochem* **122**, 498-505 (1997).
53. L. Beltrán, M. Beltrán, A. Aguado, G. Gisselmann, H. Hatt, 2-Aminoethoxydiphenyl borate activates the mechanically gated human KCNK channels KCNK 2 (TREK-1), KCNK 4 (TRAAK), and KCNK 10 (TREK-2). *Front Pharmacol* **4**, 63 (2013).
54. M. Prakriya, R. S. Lewis, Potentiation and inhibition of Ca^{2+} release-activated Ca^{2+} channels by 2-aminoethyldiphenyl borate (2-APB) occurs independently of IP_3 receptors. *J Physiol* **536**, 3-19 (2001).
55. M. V. Yelshanskaya, A. I. Sobolevsky, Ligand-binding sites in vanilloid-subtype TRP channels. *Front Pharmacol* **13**, 900623 (2022).
56. H. Shen, D. Liu, K. Wu, J. Lei, N. Yan, Structures of human $Na_V1.7$ channel in complex with auxiliary subunits and animal toxins. *Science* **363**, 1303-1308 (2019).
57. S. Hahn, S. W. Kim, K. B. Um, H. J. Kim, M. K. Park, N-benzhydryl quinuclidine compounds are a potent and Src kinase-independent inhibitor of NALCN channels. *Br J Pharmacol* **177**, 3795-3810 (2020).

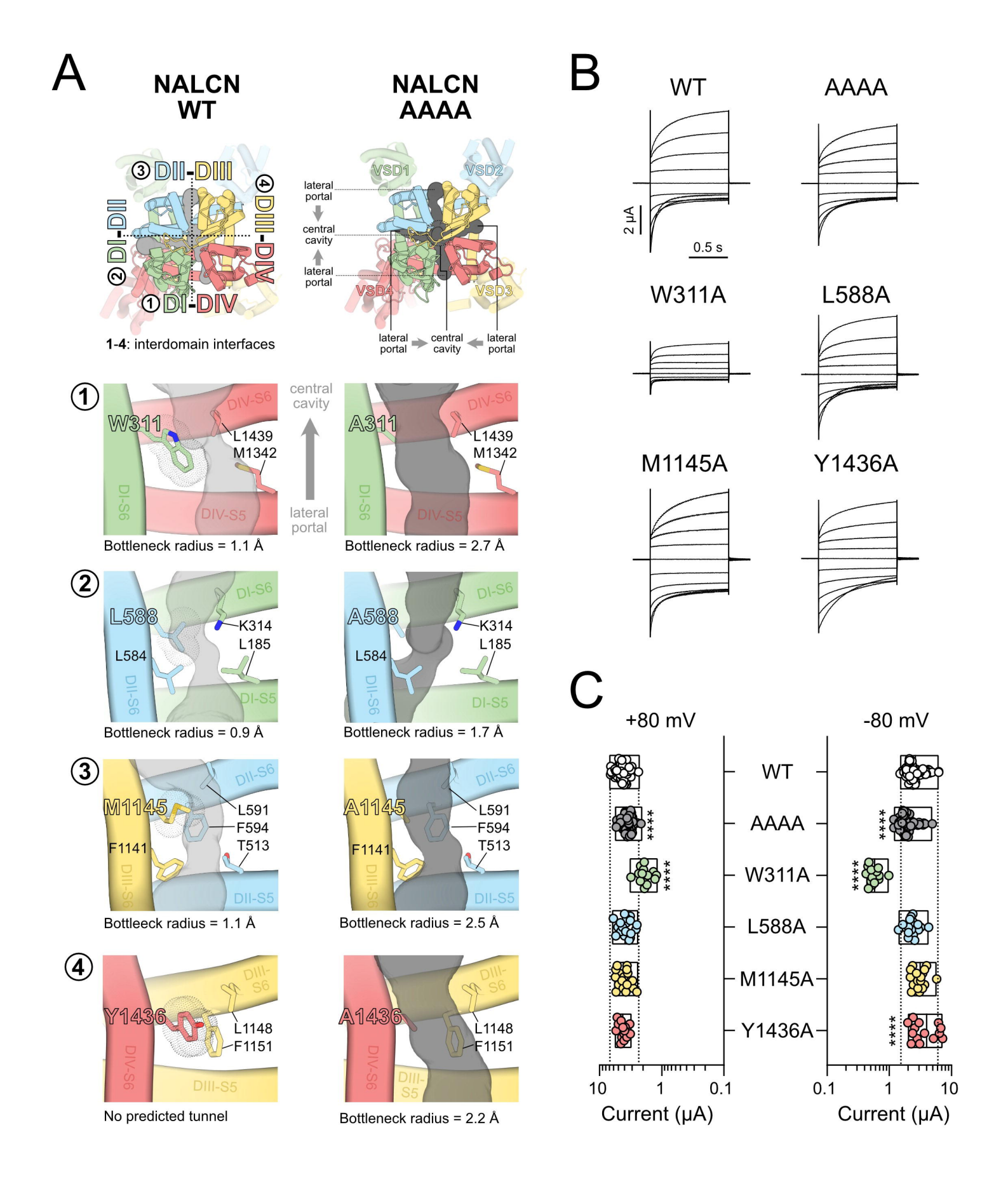
A
NALCN WT
NALCN AAAA
③ DII-DIII
④ DIII-DIV
② DI-DII
① DI-DIV
1-4: interdomain interfaces
VSD1
VSD2
VSD4
VSD3
lateral portal
central cavity
lateral portal
lateral portal
central cavity
lateral portal
①
W311
L1439
M1342
DIV-S6
DI-S6
DIV-S5
central cavity
lateral portal
A311
L1439
M1342
DIV-S6
DI-S6
DIV-S5
Bottleneck radius = 1.1 Å
Bottleneck radius = 2.7 Å
②
L588
K314
L185
L584
DI-S6
DII-S6
DI-S5
A588
K314
L185
L584
DI-S6
DII-S6
DI-S5
Bottleneck radius = 0.9 Å
Bottleneck radius = 1.7 Å
③
M1145
L591
F594
T513
F1141
DII-S6
DIII-S6
DII-S5
A1145
L591
F594
T513
F1141
DII-S6
DIII-S6
DII-S5
Bottleeck radius = 1.1 Å
Bottleneck radius = 2.5 Å
④
Y1436
L1148
F1151
DIII-S6
DIV-S6
DIII-S5
A1436
L1148
F1151
DIII-S6
DIV-S6
DIII-S5
No predicted tunnel
Bottleneck radius = 2.2 Å
B
WT
AAAA
2 µA
0.5 s
W311A
L588A
M1145A
Y1436A
C
+80 mV
-80 mV
WT
AAAA
W311A
L588A
M1145A
Y1436A
****
****
****
****
****
10
1
0.1
0.1
1
10
Current (µA)
Current (µA)

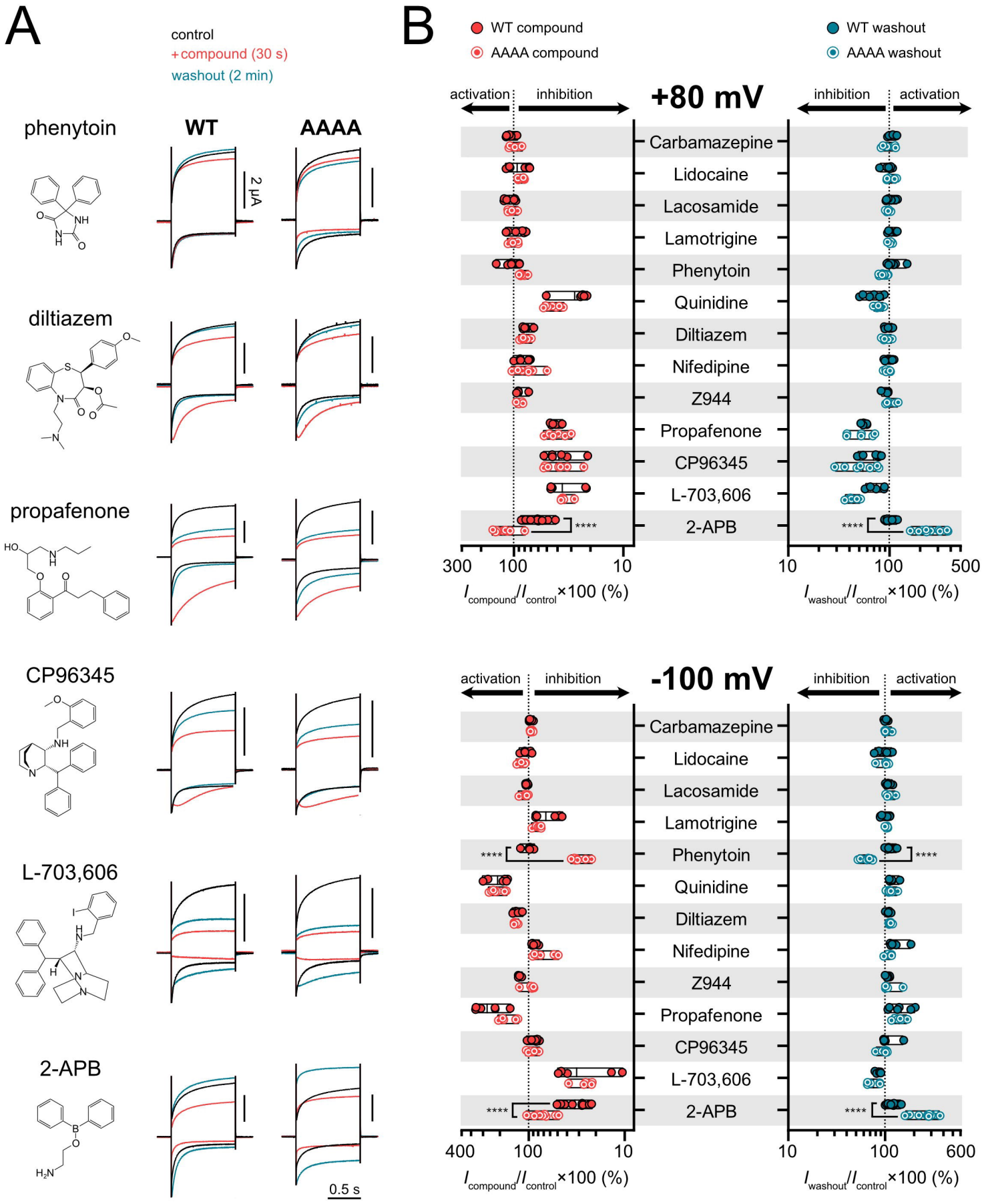
A
control
+compound (30 s)
washout (2 min)
phenytoin
WT
AAAA
2 µA
diltiazem
propafenone
CP96345
L-703,606
2-APB
0.5 s
B
WT compound
AAAA compound
WT washout
AAAA washout
activation
inhibition
+80 mV
Carbamazepine
Lidocaine
Lacosamide
Lamotrigine
Phenytoin
Quinidine
Diltiazem
Nifedipine
Z944
Propafenone
CP96345
L-703,606
2-APB
****
300
100
10
500
600
400
$I_{compound}/I_{control}$×100 (%)
$I_{washout}/I_{control}$×100 (%)
-100 mV

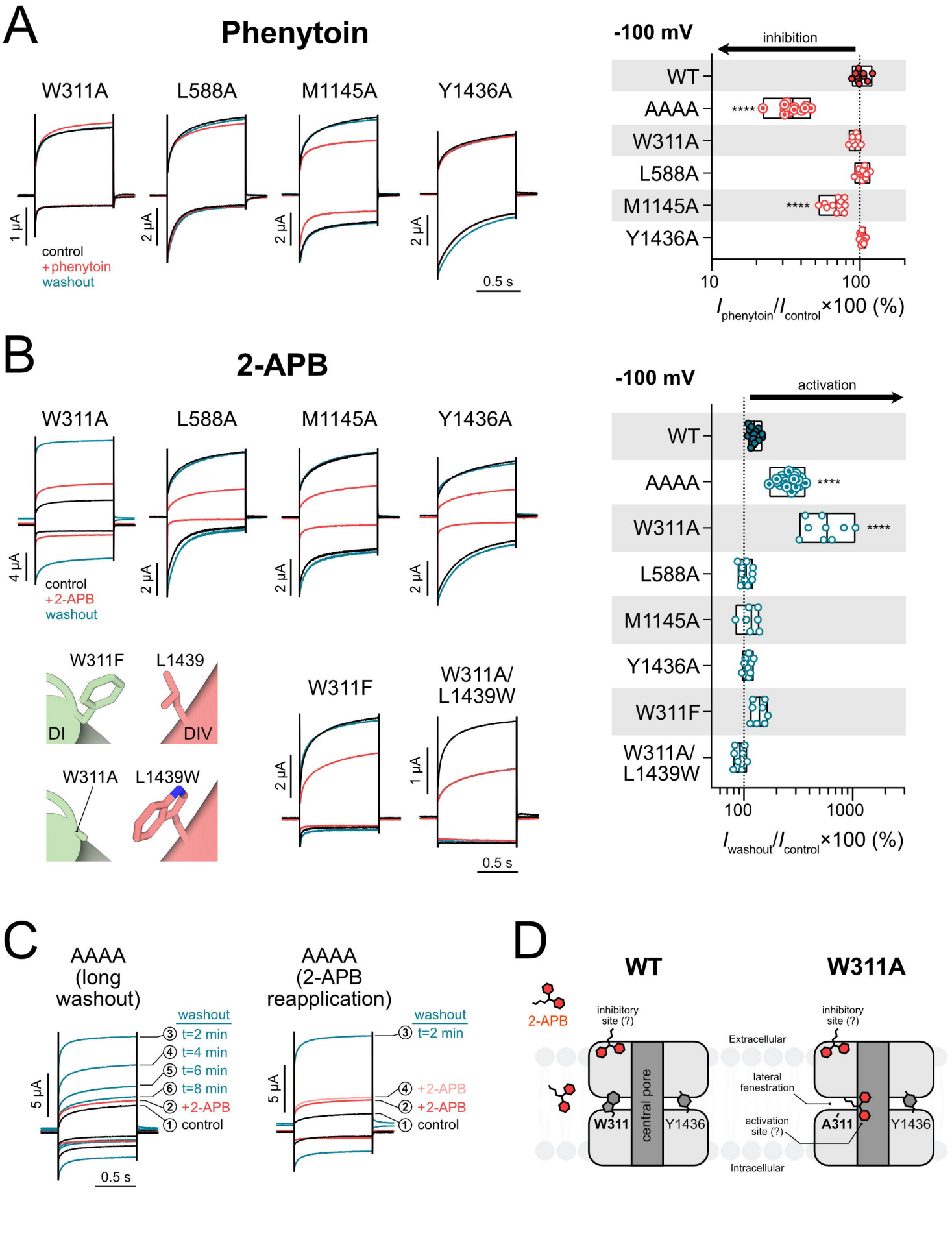
A
Phenytoin
W311A
L588A
M1145A
Y1436A
1 µA
2 µA
2 µA
2 µA
control
+phenytoin
washout
0.5 s
-100 mV
inhibition
WT
AAAA
W311A
L588A
M1145A
Y1436A
****
****
10
100
I phenytoin/I control ×100 (%)
B
2-APB
W311A
L588A
M1145A
Y1436A
4 µA
2 µA
2 µA
2 µA
control
+2-APB
washout
W311F
L1439
DI
DIV
W311A
L1439W
W311F
W311A/
L1439W
2 µA
1 µA
0.5 s
-100 mV
activation
WT
AAAA
W311A
L588A
M1145A
Y1436A
W311F
W311A/
L1439W
****
****
100
1000
I washout/I control ×100 (%)
C
AAAA
(long
washout)
AAAA
(2-APB
reapplication)
washout
③ t=2 min
④ t=4 min
⑤ t=6 min
⑥ t=8 min
② +2-APB
① control
5 µA
0.5 s
washout
③ t=2 min
④ +2-APB
② +2-APB
① control
5 µA
D
WT
W311A
2-APB
inhibitory
site (?)
central pore
W311
Y1436
Extracellular
lateral
fenestration
activation
site (?)
A311
Intracellular